V International Conference on Computational Methods for Coupled Problems in Science and Engineering
COUPLED PROBLEMS 2013
S. Idelsohn, M. Papadrakakis and B. Schrefler (Eds)

A FULLY COUPLED THERMO-HYDRO-MECHANICAL MODEL FOR THE ANALYSIS OF THE LINING BEHAVIOR OF UNDERGROUND CAVERNS IN AN AA-CAES SYSTEM

ANIS EL MURR *, FAOUZI HADJ-HASSEN, AHMED ROUABHI AND MICHEL TIJANI
Department of Geosciences, MINES-ParisTech, 35 rue Saint-Honoré, 77305 Fontainebleau, France
anis.el_murr@mines-paristech.fr

Key words: thermo-hydro-mechanical coupling, underground storage, AA-CAES.

Abstract. With the worldwide demand for electricity, renewable energy is attracting increasing attention. As this energy has an intermittent character, large-scale storage technologies are necessary. One of the most promising systems is the advanced adiabatic compressed air energy storage (AA-CAES) in underground lined rock caverns. The high cyclic thermal and mechanical loadings involved in the system can disturb the surrounding geological barrier and thus lead to the failure of the system. The implementation of a special lining capable of limiting the thermal losses, reducing the air leakage and ensuring the caverns stability, is therefore required.

This paper presents the governing equations for fully coupled thermo-hydro-mechanical (THM) processes in saturated deformable media filled with dry air which characterize the conditions of the storing system. The assumptions used to simplify the equations are discussed and the neglected terms are underlined. These equations take into account the dependence of thermal conductivity on temperature, convection and heat compression. The air properties are derived using Helmholtz energy. A comprehensive comparison between the proposed model and a simple THM model based on constant parameters, ideal gas and conductive flux is made in order to emphasize the phenomena that could occur and their influences. Finally, thermo-hydro-mechanical simulations of the different lining materials are carried out to analyze the advantages and the drawbacks of each solution.

1 INTRODUCTION

The use of fossil fuel reserves to produce electricity presents many drawbacks; it is a finite resource and releases CO_2 which is the major cause of global warming [1,2]. Renewable energy is becoming more and more widespread, but it has two major problems: the first one is the big distance between energy resources and energy demand, which causes additional significant costs; the second one is the stochastic nature of this source [3]. Large-scale energy storage systems can solve these problems. Two systems are known to be the best: the pumped hydroelectric storage (PHS) and the compressed air energy storage (CAES) because of their high cost effectiveness. (PHS) system has a high cost and requires a suitable topography, which is rare; so, the (CAES) is the best promising technology to store energy [1].

The first storage station using an underground compressed air reservoir was a 290MW unit built in Huntorf, Germany, in 1978. It consists of two salt caverns with a total volume of 310,000m^3 [4,5] and an operating pressure between 4.8MPa and 6.8MPa. The second was a 110MW unit built in MacIntosh, USA. It consists of one salt cavern with a volume of 560,000m^3 and an operating pressure between 4.5MPa and 7.4MPa [1]. In the USA, a big interest is given nowadays to the construction of this type of plants; the largest is the 2,700 MW Iowa Stored Energy Park [6,7,8].

This system converts the off-peak electricity taken from the grid to a compressed air and stores it in an underground cavern. Then the air is used to drive a turbine to generate electricity when needed. After the compression stage, this system uses an inter-cooler and an after-cooler in order to reduce the air temperature, which leads to the decrease of the thermal stresses on the cavern walls and the reduction of the storage volume. Fuel is combusted then inside the turbine to increase the air temperature and thus its efficiency.

The advanced adiabatic compressed air energy storage (AA-CAES) is a modification of the (CAES) system; the innovative idea is that the heat generated during compression is stored in a thermal energy storage unit (TES) and recovered in the expansion phase (Fig. 1). AA-CAES is then more efficient and less damaging to the environment (no CO_2 emissions).

The high cyclic thermal and mechanical loadings applied to the TES walls (temperature up to 550^0C and pressure up to 15MPa) would damage the surrounding rock mass and then lead to the failure of the system. This type of loading has never been treated in a gas storage application. To solve this problem, the implementation of a special lining, which role is to help the rock mass hold the gas pressure, to ensure a sufficient thermal isolation and to reduce the air leakage to an acceptable rate, is therefore necessary.

Two major studies have been held in Sweden to study natural gas storage in lining rock caverns. In Grängesberg and in Skallen [9,10,11], the caverns were constructed in fractured granite and lined by concrete and steel. As for CAES, a study was made on a former coal mine in Hokkaido Prefecture [3], Japan. The lining consists of 0.7 m concrete filled with a synthetic rubber seal. A recent study presented in [3,8] explored the potential of CAES in lined rock caverns at shallow depth (100 m), and has shown its feasibility from a leakage and energy-efficiency perspective. The lining consists of 1 m concrete.

In the experiences stated above, the steel and the synthetic rubber have a sealing function, the concrete has the pressure transmitting function and the rock mass has the pressure absorbing function.

The Preliminary simulations for the (TES) lined with steel and concrete showed a failure of the system. The stress criteria indicate that the materials will break because of the highly compressive thermal stresses generated by the high temperature. Thus, the implementation of a cooling system in the front wall of concrete layer is quite necessary to prevent the instability of the concrete and of the rock mass. Furthermore, an insulating material is added in front of the concrete layer to ensure thermal insulation.

The understanding of the interaction of different physics in the system is necessary to design the lining of the TES. Thus, a fully Thermo-Hydro-Mechanical model in saturated deformable media filled with dry air is presented. This model takes into consideration the dependency of the thermal conductivity of the materials and dry air properties on the temperature, convection and heat compression. A comparison with a simple THM model

(constant parameters, conductive flux) is made and a geomechanical analysis of the TES lining is carried out in order to optimize the design.

2. GENERAL BALANCE EQUATIONS

In the following derivations, we consider a deformable porous media fully saturated with air, and it is considered to be in local thermal equilibrium with the solid phase. A macroscopic approach is applied, meaning that the porous medium can be treated as a continuum where volume-averaged quantities replace local ones. The balance equations are derived by considering the conservation laws of two phases (solid and fluid) and by summing the contribution of both phases.

2.1 Mass balance equation

The Eulerian forms of mass balances of both phases are given by:

$$\frac{\partial \emptyset \rho_f}{\partial t} + \nabla.(\emptyset\, \rho_f V_f) = 0 \quad \textbf{(1)}$$

$$\frac{\partial (1-\emptyset)\rho_s}{\partial t} + \nabla.((1-\emptyset)\, \rho_s V_s) = 0 \quad \textbf{(2)}$$

Where $\emptyset$ is the porosity of the porous media, ρ_f and ρ_s are the mass per unit of volume for the fluid and the solid respectively. V_f and V_s are the velocities of the fluid and the solid respectively with respect to a fixed reference. Developing eq.(1) and eq.(2) leads to the total mass balance equation:

$$\emptyset \frac{\partial \rho_f}{\partial t} + \rho_f \left[\frac{\partial \varepsilon_v}{\partial t} + \frac{(1-\emptyset)}{\rho_s}\frac{D\rho_s}{D^s t}\right] = -\nabla.\, q_{rf} \quad \textbf{(3)}$$

where ε_v is the skeleton volumetric strain, q_{rf} is the flux density vector with respect to the solid particles, and $\frac{D}{D^s t}$ is the co-moving time derivative for tracking the motion of a solid particle along its trajectory.

2.2 Momentum balance

In the absence of inertia forces, the law of conservation of linear momentum is given by :

$$\nabla.\sigma + \rho_m g = 0 \quad \textbf{(4)}$$

where σ is the total stress tensor, g is a vector representing the acceleration of gravity and ρ_m is the average density of the mixture:

$$\rho_m = (1-\emptyset)\rho_s + \emptyset\rho_f \quad \textbf{(5)}$$

2.3 Energy balance

Neglecting the dissipation of energy due to the viscosity of the air and the irreversible energy dissipation in the skeleton, and any heat transfer caused by the solid displacement, the energy balance equation for both phases is then given by:

$$(1-\emptyset)\rho_s C_{p_s}\frac{\partial T_s}{\partial t} = -\nabla.q_s \quad (6)$$

$$\emptyset\rho_f C_{p_f}\left(\frac{\partial T_f}{\partial t}+\rho_f C_{p_f} v_{rf}.\nabla T\right) = \frac{\partial p}{\partial t} - \nabla.q_f \quad (7)$$

where q_s and q_f are the conductive fluxes of the solid and the fluid respectively, C_{p_s} and C_{p_f} are the isobaric heat capacities of the solid and the fluid respectively and v_{rf} is the velocity of the fluid particles with respect to the solid.

3. GENERAL CONSTITUTIVE EQUATIONS

3.1 Hydraulic

Neglecting any influence of thermal gradient on the air flux (thermo-osmosis) and any change in permeability due to air slippage (Klinkenberg effect), the mass flux could be written then in the following form:

$$q_{rf} = -\rho_f \frac{k_h}{\mu_f}(\nabla p - \rho_f g \nabla z) \quad (8)$$

where k_h is the intrinsic permeability of the media, μ_f is the dynamic viscosity of the fluid and z is the elevation.

The thermodynamic state of the air, considered as an homogenous fluid resulting from the mixture of different gases, is described by the couple (p,T) . The rate of change of air density is given by:

$$\frac{\dot{\rho}_f}{\rho_f} = \beta_f \dot{p} - 3\alpha_f \dot{T} \quad (9)$$

where β_f is the compressibility modulus of the fluid and α_f is the linear thermal expansion coefficient (both are function of the couple (p,T)). For an ideal gas, these parameters are given by:

$$\beta_f = \frac{1}{p} \quad (10)$$

$$\alpha_f = \frac{1}{3T} \quad (11)$$

Since we are dealing with a wide range of temperatures (up to 550℃) and pressures (up to 15MPa), the assumption that the fluid is an ideal gas may not be sufficient. Thus, using a state law for dry air proposed by Lemmon [12] would be a better approach. This law uses the Helmholtz free energy given by:

$$f(\rho,T) = \ln(\delta) + \sum_{i=1}^{5} N_i \tau^{i-4} + N_6\tau^{1.5} + N_7\ln(\tau) + N_8\ln(1-e^{-N_{11}\tau}) + N_9\ln(1-e^{-N_{12}\tau}) + N_{10}\ln\left(\frac{2}{3}+e^{N_{13}\tau}\right) + \sum_{i=1}^{10} N_k \delta^{i_k}\tau^{j_k} + \sum_{k=11}^{19} N_k\,\delta^{i_k}\tau^{j_k}e^{-\delta^{l_k}} \quad (12)$$

where $\delta = \frac{\rho}{\rho_0}$, $\tau = \frac{T_0}{T}$ and (ρ_0, T_0) a state of reference. The coefficients N_i, N_k, i_k, j_k and l_k are constants. Knowing this thermodynamic potential, all the thermodynamic properties of dry air can be easily computed. A comparison between the two models described above was carried out. Fig. 2 (a, b) shows β_f and C_{p_f} as a function of pressure and for a fixed value of temperature (200°C). For both parameters, we note a relative difference going up to 10%. Fig.

3 shows α_f as a function of temperature and for a fixed value of pressure (5MPa). Again, a relative difference going up to 14% is remarked. For accuracy purposes, Lemmon's model is used. Fig. 4 (a, b, c) shows C_{p_f} , α_f and ρ_f as a function of temperature and for different pressures according to this model.

3.2 Thermal

Neglecting any heat flux caused by a pressure gradient, the heat conduction flux could be written as:

$$q = -\lambda_m \nabla T \tag{13}$$

where q is the sum of the thermal conductive heat flux of the fluid and the thermal conductive heat flux in the solid, λ_m is the apparent macroscopic thermal conductivity over all phases; it is expressed as:

$$\lambda_m = (1 - \emptyset)\lambda_s + \emptyset\lambda_f \tag{14}$$

Experimental results showed that the thermal conductivity for the insulation material and for the refractory concrete is a linear function of temperature. Details are showed in table 1.

3.3 Mechanical

Adopting a small strain approach, the total strain tensor ε and the volumetric strain are given by

$$\varepsilon = \frac{1}{2}(\nabla \mathrm{u} + (\nabla \mathrm{u})^{\mathrm{t}}) \tag{15}$$

$$\varepsilon_v = \nabla . \mathrm{u} \tag{16}$$

where u is the displacement vector and t denotes the transpose of the tensor. The effective stress law for fully saturated media is given by [13]:

$$\sigma = \sigma' - \boldsymbol{I}p \tag{17}$$

where σ' is the macroscopic effective stress tensor given by:

$$\sigma' = D : (\varepsilon - \varepsilon_T - \varepsilon_p) \tag{18}$$

where D is the tangential stiffness matrix, and ε is the total solid skeletal strain tensor, ε_T is the thermal strain caused by temperature increase; it is given by:

$$\varepsilon_T = \alpha_d \boldsymbol{I} \Delta T \tag{19}$$

where α_d is the drained linear thermal expansion coefficient and ε_p is the strain caused from compression of grains by internal hydrostatic fluid pressure, it is given by:

$$\varepsilon_p = -\frac{\boldsymbol{I}\Delta p}{3k_g} \tag{20}$$

where k_g is the bulk modulus of solid grains. The constitutive equation required to calculate the changes in solid grains, for small changes in grain density, is given by [14]:

$$\frac{\rho_s}{\rho_{s0}} = 1 + \frac{p-p_0}{k_g} - \alpha_g(T - T_0) - \frac{trace(\sigma' - \sigma'_0)}{(1-\emptyset)3k_g} \quad \textbf{(21)}$$

where α_g is the linear thermal expansion coefficient of solid grains and the subscript 0 labels a reference state.

4. FINAL EQUATIONS

4.1 Hydraulic

Combining the aforementioned balance and constitutive equations and neglecting the terms $v_f.\nabla p$, $v_f.\nabla T$ and $v_f.\nabla \rho_f$, we obtain:

$$\frac{1}{M}\frac{\partial p}{\partial t} - \alpha_m \frac{\partial T}{\partial t} + b\frac{\partial \varepsilon_v}{\partial t} = -\frac{1}{\rho_f}\nabla.(-\rho_f \frac{k_h}{\mu_f}(\nabla p - \rho_f g \nabla z)) \quad \textbf{(22)}$$

where:

$$\frac{1}{M} = \emptyset\beta_f + \frac{b-\emptyset}{k_g} \quad \textbf{(23)}$$

is an isothermal storage coefficient and

$$\alpha_m = 3\emptyset\alpha_f + (1-\emptyset)\alpha_g - (1-b)\alpha_d \quad \textbf{(24)}$$

is the linear differential thermal expansion coefficient. Note that b is the well-known Biot coefficient.

4.2 Thermal

Using the assumptions of local thermal equilibrium, neglecting $v_s.\nabla T$, $v_s.\nabla p$ and $v_f.\nabla p$ and combining eq. (6), (7) and (11), we obtain:

$$(\rho C_p)_m \frac{\partial T}{\partial t} + \rho_f C_{p_f} v_{rf}.\nabla T - \frac{\partial p}{\partial t} = -\nabla.(-\lambda_m \nabla T) \quad \textbf{(25)}$$

where:

$$(\rho C_p)_m = (1-\emptyset)\rho_s C_{p_s} + \emptyset\rho_f C_{p_f} \quad \textbf{(26)}$$

4.3 Mechanical

Combining eq. (4), (15), (16) and (17) and neglecting gravity forces, we obtain the well-known equilibrium equation:

$$G\nabla^2 u + (G+\lambda)\nabla(\varepsilon_v) - b\nabla p - 3\alpha_d k_d \nabla T = 0 \quad \textbf{(27)}$$

where G and λ are Lame's elasticity constants.

5. NUMERICAL MODEL

5.1 Model geometry

The cavity is a vertical cylinder with a 20 m diameter, a 50 m height, a domed roof and rounded invert. In order to simplify the simulations, the cavity is represented by a 1D axisymmetric model neglecting the effect of gravity and the cavity extremities. The simulations were carried out on two basic configurations shown in Fig. (2, 3).

5.2 Materials model

Since no information is available on the mechanical behavior of these materials under high temperature and high pressure, an elastic behavior was assumed. The thermo-hydro-mechanical properties adopted for these materials are given in detail in table 1.

Table 1: Thermo-hydro-mechanical properties.

Property	Refractory concrete	Insulation material	Concrete	Granite
Young's modulus(GPa)	5	1	20	35
Poisson ratio	0.2	0.25	0.2	0.2
Uniaxial compressive strength (MPa)	40	2	30	60
Thermal conductivity (W/m/K) $\lambda = aT + b$; (a, b), where T is in °C	(0.0005, 3.4)	(0.0001, 0.36)	1.75	2.5
Heat capacity (J/kg/K)	950	1100	880	970
Permeability (m^2)	10^{-19}	10^{-11}	10^{-18}	10^{-15}
Drained linear thermal expansion coefficient (1/K)	0.78×10^{-5}	0.6×10^{-5}	1×10^{-5}	0.9×10^{-5}
Biot's coefficient	0.9	0.9	0.9	0.9

5.3 Initial and boundary conditions

The initial stress regime in the granite rock is assumed to be isotropic and equal to 3.24 MPa. The excavation of the cavern is modeled using the convergence-confinement method. The mechanical load comprises 3 main phases: an increase of the pressure during 5 days from 0 to 5.2 MPa, then the pressure is maintained constant during 46 days before performing 9 cycles of 24 hours for each of them. As shown in Fig. 7a, the pressure is cycling between 4 and 8 MPa. In the same way, the thermal load also comprises three main phases: an increase of temperature during the first 5 days from 12.5 to 370°C, then the temperature is held constant during 46 days, followed by 9 cycles oscillating between 170 and 470°C of 24 hours for each of them (Fig. 7b). The limit of the model within the granite layer was defined sufficiently far to ensure that no radial displacement will occur. The numerical code used is COMSOL MULTIphysics. Coupling conduction and convection with poroelasticity was carried out by the earth science module.

6. RESULTS

Preliminary simulations showed that the deformation caused by the mechanical load does not significantly affect the hydrostatic pressure field, thus the predominant coupling is thermo-hydraulic. This means that once the temperature and the pressure fields are computed, they are provided to the mechanical module in order to compute the stresses.

6.1 Thermo-hydraulic coupling

As mentioned in the introduction, comparisons were made between the model presented above and a simple THM model (constant parameters, no convection, no heat compression…). For this purpose, we have chosen 24 significant dates in one cycle and showed differences in temperature and in hydrostatic pressure between both models. Fig.8a shows that a difference from -12 to 10°C in the temperature field could occur. This difference does not significantly affect the daily thermal losses which are equal to 0.56% for the first configuration and to 0.64% for the second one. As for the pressure field, the comparison for the first configuration did not show any significant difference (daily losses: 0.18%), but in the second one, the difference could reach 1,15MPa as shown in Fig. 8b. Furthermore, the concrete layer is sufficient to maintain daily air losses below 1%. No significant difference is noted between both models from an air leakage point of view.

6.2 Stability analysis

The stability of the cavity is analyzed using the Mohr-Coulomb's failure criterion given by:

$$f(\sigma_1', \sigma_2', \sigma_3') = k\sigma_1' - \sigma_3' \leq R_c \quad \textbf{(28)}$$

where σ_1', σ_2' and σ_3' are the effective principal stresses, k is the passive pressure coefficient ($k = 3$ and corresponds to a friction angle of 30°) and R_c is the uniaxial compressive strength. The materials are considered to support no tensile stress.

$$\sigma_1' \leq 0 \quad \textbf{(29)}$$

The Mohr-Coulomb's criterion shows that the proposed model is more critical than the classic one, and that there is no failure in shear for both configurations ($S = 1$ for the first configuration and $S = 2$ for the second configuration, where S is the safety factor, Fig. 9 (a, b)). A tensile stress might occur in the refractory concrete due to the term $\alpha_m \frac{\partial T}{\partial t}$ in the final hydraulic equation. The tensile stress is not only dependent on the linear thermal expansion coefficient of air, but also on the Biot's coefficient, the more this coefficient is close to 1, the more the stresses are higher. This result requires a deep understanding of the poroelastic behavior of the refractory concrete and an accurate measurement of the Biot's coefficient.

7. CONCLUSION

A fully coupled THM model has been developed to study the lining behavior in a TES cavern of an AA-CAES system. Comprehensive comparisons were made with a classic THM

model in order to point out the major differences. The daily heat losses and daily air losses are below 1% for both lining configurations, which is acceptable. It has also been shown that there is no failure by excess of shear; in order to increase the safety factor especially in the first configuration ($S = 1$), the use of thermal joints (inserted between the blocs of the insulation material) that compensate the thermal expansion and thus reduce thermo-mechanical stresses is therefore necessary. Simulation also showed that a tensile stress could occur. A detailed study of the poroelastic properties of the refractory concrete is needed.

ACKNOWLEDGEMENT

This work was performed under the project SEARCH. The authors express their thanks to the French National Research Agency (ANR) for sponsoring this program as well as to the partners of this project GDF SUEZ, St Gobain and CEA/Liten.

REFERENCES

[1] De Samaniego Steta, F. Modeling of an Advanced Adiabatic Compressed Air Energy Storage(AA-CAES) Unit and an Optimal Model-based Operation Strategy for its Integration into Power Markets. Master Thesis PSL1003.

[2] Rogner, H-H. An assessement of world hydrocarbon resources, Annu. Rev. Energy Environ. 1997. 22:217–62

[3] Rutqvist, J., MokKim, H., WooRyu, D., HoSynn, J. and KyongSong, W. Modeling of coupled thermodynamic and geomechanical performance of underground compressed air energy storage in lined rock caverns. International Journal of Rock Mechanics & Mining Sciences 52 (2012) 71–81.

[4] Ibrahim, H.. Ilinca, A. and Perron, J. Energy storage systems—Characteristics and comparisons. Renewable and Sustainable Energy Reviews 12 (2008) 1221–1250.

[5] Succar, S. and Williams, R.H. Compressed air energy storage: Theory, resources, and applications for wind power. Technical report, Princeton Environmental Institute, Princeton, New Jersey, April 2008

[6] http://www.scotland.gov.uk/Publications/2010/10/28091356/4

[7] Fertig, E. and Apt, J. Economics of compressed air energy storage to integrate wind power: A case study in ERCOT. Energy Policy 39 (2011) 2330–2342

[8] Kim, H. M., Rutqvist, J., Ryu, D.W., Synn, J. H. and Song, W.K. Coupled Nonisothermal, Multiphase Fluid Flow and Geomechanical Analysis of Underground Compressed Air Energy Storage (CAES) in Lined Rock Caverns.

[9] Johansson J. High pressure storage of gas in lined rock caverns- cavern wall design principles. licentiate thesis, division of soil & rock mechanics. Stockholm: Royal Institute of Technology; 2003139pp.

[10] Glamheden, R and Curtis, P. Excavation of a cavern for high-pressure storage of natural gas. Tunnell Undergr Space Tech 2006:56–67.

[11] Mansson, L., Marion and P., Johansson, J. Demonstration of the LRC gas storage concept in Sweden. In. Proceedings of the world gas conference. Paperno. 2.2CS.03. Amsterdam;5–9June 2006.

[12] Lemmon, E. W., Jacobsen, R.T. Penoncello, S.G. and Friend, D.G. 2000 : Thermodynamic properties of air and mixtures of nitrogen, argon and oxygen from 60 to 2000 K at pressures to 2000 MPa. J. Phys. Chem. Ref. Data, 29, 331-362.

[13] Rutqvist, J., Börgesson, L., Chijimatsuc, M., Kobayashic, A., Jingd, L., Nguyene T.S., Noorishada, J. and Tsanga C.-F. Thermohydromechanics of partially saturated geological media:governing equations and formulation of four finite element models. International Journal of Rock Mechanics & Mining Sciences 38 (2001) 105±127.

[14] ABAQUS Manuals-version 5.5. Pawtucket, Rhode Island, USA:Hibbitt, Karlson and Sorensen Inc.

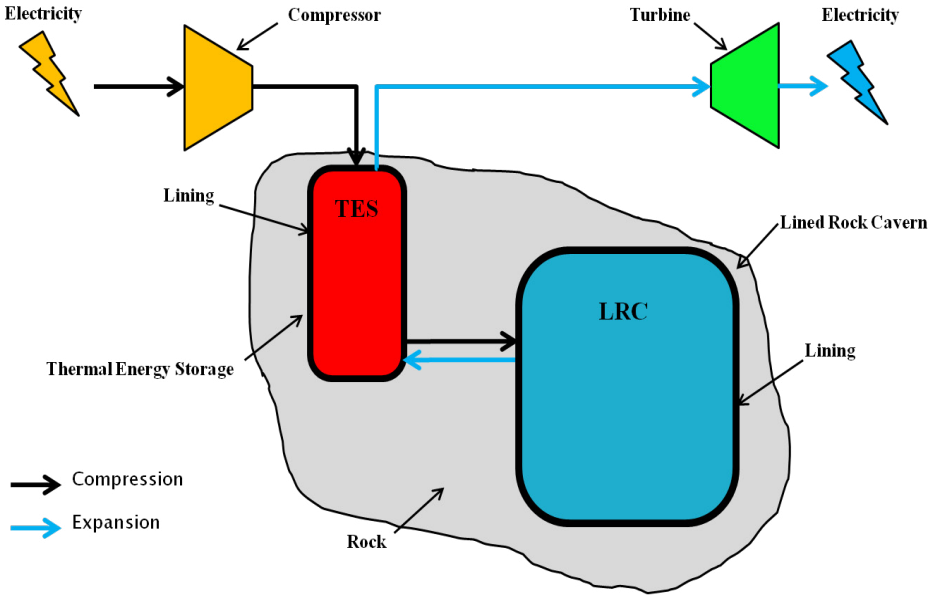

Figure 1: The concept of an AA-CAES system

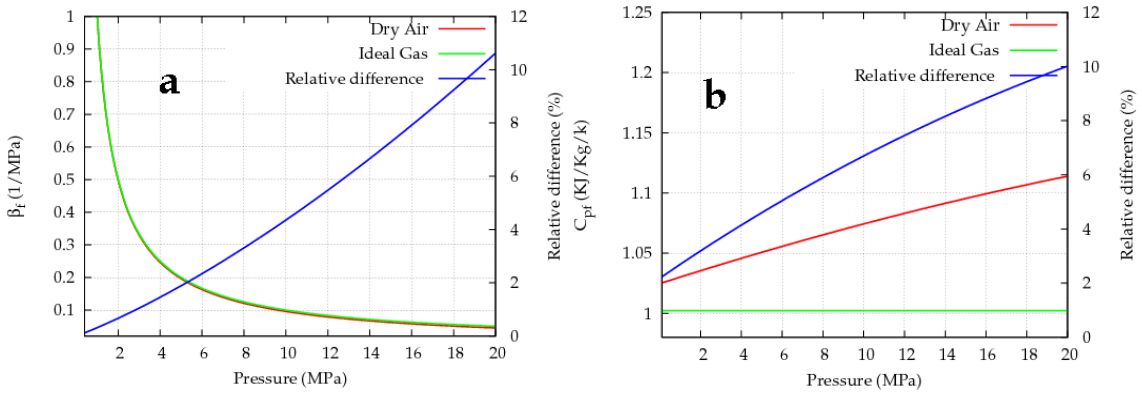

Figure 2 (a, b): β_f and C_{p_f} as a function of pressure and for a fixed value of temperature (200°C).

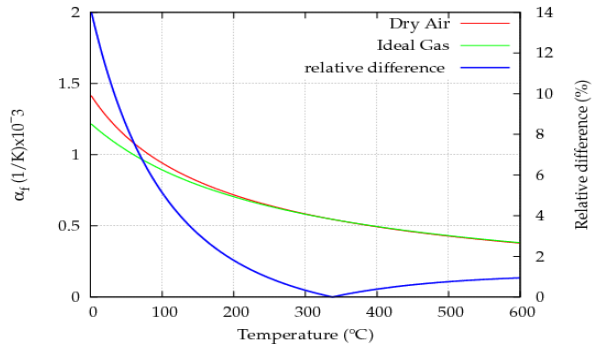

Figure 3: α_f as a function of temperature and for a fixed value of pressure (5MPa).

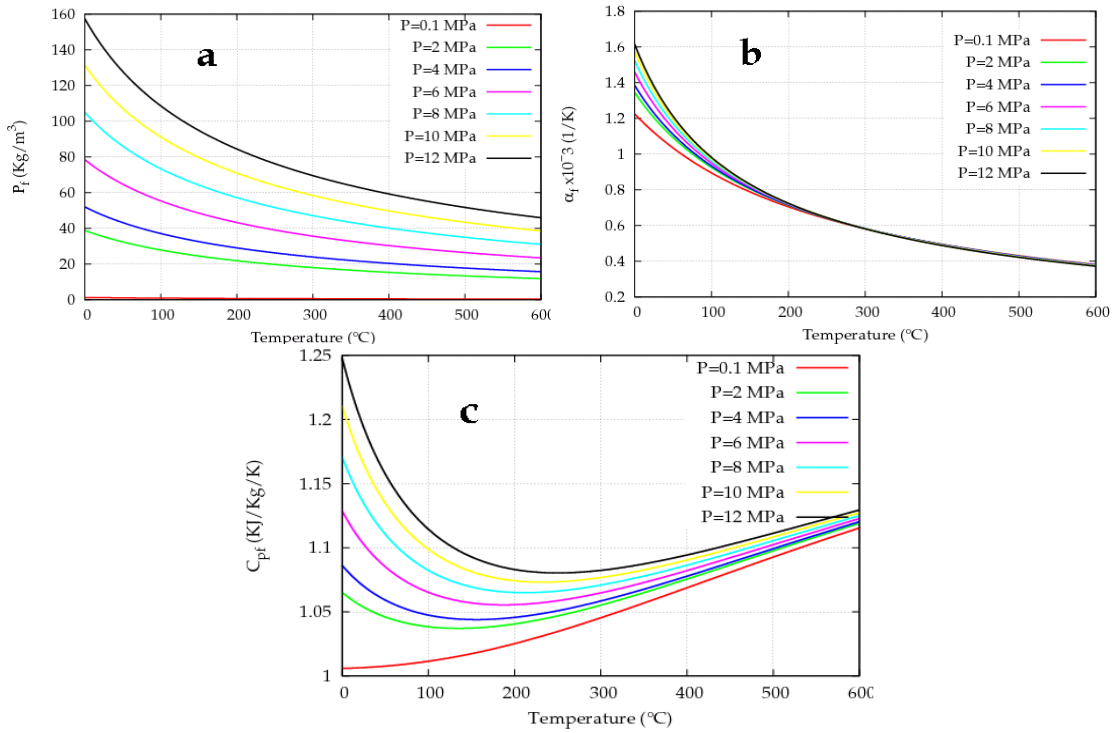

Figure 4 (a, b, c): C_{p_f}, α_f and ρ_f as a function of temperature and for different pressures according to Lemmon's model[12].

Figure 5: Configuration 1: insulation material + cooling system (in red) + concrete+ granite.

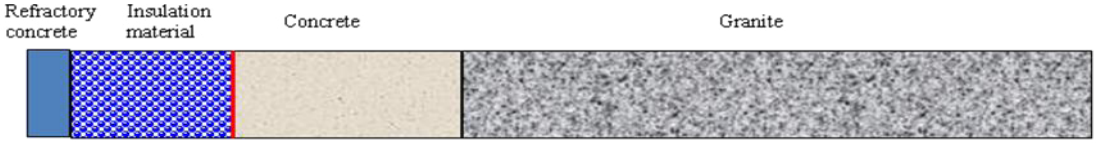

Figure 6: Configuration 2: refractory concrete + insulation material+ cooling system + concrete+ granite.

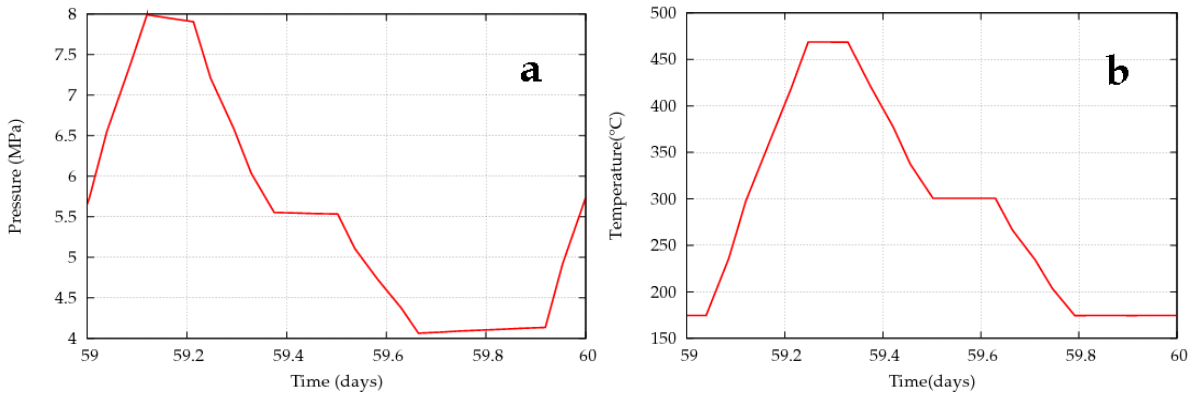

Figure 7: Mechanical (a) and thermal (b) loadings for one cycle (24 hours).

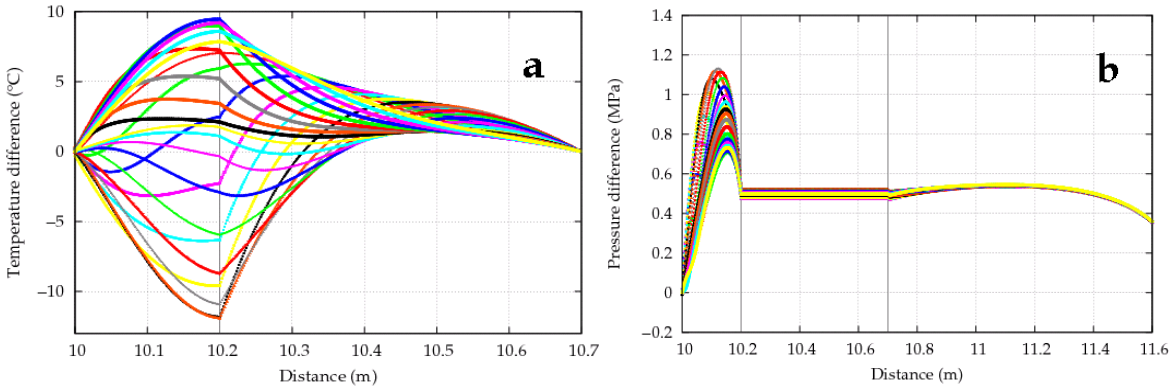

Figure 8: Comparison with a classic THM model, differences for temperature (a) and pressure (b) between both models for the second configuration.

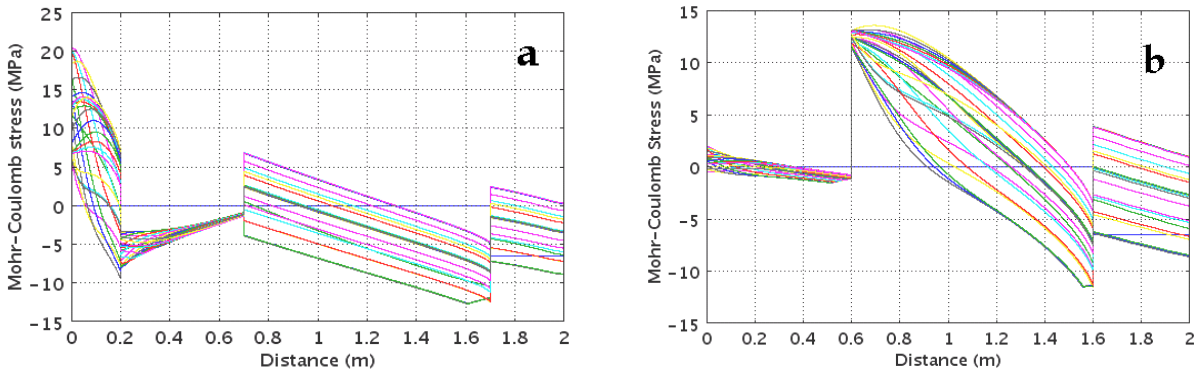

Figure 9 (a, b): Mohr-Coulomb's stress criterion for both configurations.